C1

NACA

RESEARCH MEMORANDUM

FLUTTER AND DIVERGENCE OF RECTANGULAR WINGS OF VERY LOW ASPECT RATIO

By Robert W. Fralich, John M. Hedgepeth, and W. J. Tuovila

Langley Aeronautical Laboratory
Langley Field, Va.

NATIONAL ADVISORY COMMITTEE FOR AERONAUTICS

WASHINGTON

June 28, 1957

NACA RM L57F24

NATIONAL ADVISORY COMMITTEE FOR AERONAUTICS

RESEARCH MEMORANDUM

FLUTTER AND DIVERGENCE OF RECTANGULAR WINGS OF VERY LOW ASPECT RATIO

By Robert W. Fralich, John M. Hedgepeth, and W. J. Tuovila

SUMMARY

Slender-body aerodynamic theory is used in conjunction with thin-plate theory in the flutter analysis of low-aspect-ratio rectangular wings of constant thickness when chordwise variations of deflections are considered. The spanwise variation of deflection is given by a parabola, and the chordwise variation is allowed complete freedom. The results show the variation of flutter speed and mode shape with aspect ratio. Comparisons are made with results obtained by approximating the chordwise deflection shape by the first few terms of a power series. Comparisons with some preliminary experimental results are also included.

INTRODUCTION

The prediction of flutter of wing and tail surfaces of very low aspect ratio is a problem of some concern to aircraft designers. The difficulties in the flutter analysis of such surfaces are mainly connected with the presence of large amounts of chordwise curvature in the flutter mode. It is of interest to investigate the complexity of the chordwise deflection shape at flutter and to determine to what degree of accuracy the chordwise deflection must be represented in order to obtain good results. This paper is concerned with the flutter behavior, both theoretical and experimental, of the simple low-aspect-ratio configuration shown in figure 1. The analysis is similar to that of reference 1, which treated the static divergence behavior of the same configuration.

SYMBOLS

x,y,z	coordinate system (see fig. 1)
$w(x,y,\tau)$	wing deflection, positive in z-direction

V	free-stream velocity
t	wing thickness
c	wing chord
s	wing semispan
τ	time
$F(x,\tau)$	chordwise deflection shape
q	dynamic pressure, $\frac{\rho V^2}{2}$
E	Young's modulus of elasticity
ρ	free-stream density of fluid
ρ_m	density of material
T	period of oscillation
M	Mach number
$\varphi(x,y,z,\tau)$	perturbation-velocity potential
λ	flutter-speed parameter, $\frac{5\pi}{4}(1 - \mu^2)\frac{q}{E}\frac{s^3}{t^3}$
K	flutter-frequency parameter, $\omega\sqrt{\frac{\rho_m t s^4}{D}}$
ϵ	mass-ratio parameter, $\frac{\pi}{2}\frac{\rho s}{\rho_m t}$
μ	Poisson's ratio (taken as 1/3 in all computations)
D	plate stiffness in bending, $Et^3/12(1 - \mu^2)$
ω	flutter frequency

THEORETICAL APPROACH

The configuration analyzed in this paper consists of a rectangular plate of constant thickness cantilevered from a rigid wall. (See fig. 1.)

This plate may be thought of as representing one-half of a wing with a chord c and a semispan s. The plate is located in a fluid flow with a free-stream velocity V. The deflection shape of such a low-aspect-ratio plate can be expected to vary in a much more complicated manner in the chordwise direction than in the spanwise direction. For this reason the deflection w is assumed to vary as $w(x,y,\tau) = y^2F(x,\tau)$, where the spanwise deflection is given by a simple parabola and the chordwise variation F of the deflection is an arbitrary function of the chordwise coordinate x and time τ. The distortions of the plate are found through the use of ordinary thin-plate theory. The aerodynamic loadings are found most simply by using slender-body aerodynamic theory. In this theory streamwise perturbations are neglected in comparison with perturbations in the crossflow direction. The use of this approximate aerodynamic theory simplifies the aeroelastic problem to the extent that an exact solution is possible. A brief description of the analysis and the resulting equations are given in the appendix.

RESULTS AND DISCUSSION

Some results are given by the boundaries shown in figure 2. The ordinate is the dynamic-pressure parameter $\frac{q/E}{(t/s)^3}$, in which q is the dynamic pressure, E is Young's modulus of elasticity for the plate, and t/s is the ratio of thickness to semispan. The abscissa is the ratio of chord to semispan c/s. The variation of the dynamic-pressure parameter for flutter with the ratio of chord to semispan is dependent upon the mass-ratio parameter $\frac{\rho s}{\rho_m t}$ in which $\frac{\rho}{\rho_m}$ is the ratio of air density to plate density. The flutter boundaries are given for two values of mass-ratio parameter; the region above a particular boundary is unstable while that below is stable. Also shown is the result for static divergence obtained from reference 1. This result, which is, of course, independent of the mass ratio, is indicated by a single curve. Note that divergence is less critical than flutter for these particular mass ratios. Note also that, for the higher mass ratio, the flutter boundary consists of a series of loops approaching a constant value of dynamic-pressure parameter. The lower curve also has this characteristic; however, the loops are so elongated in this case that only one can be seen in this figure.

The kind of flutter mode shapes obtained from the analysis is shown in figure 3. The top set of curves shows the components of tip deflection which are in phase and out of phase with the maximum leading-edge deflection for a value of c/s corresponding to the tick mark on the bottom of the first loop on the flutter boundary in figure 2. The

tip deflection is given when the leading edge has its maximum amplitude and at one-quarter of a period later when the leading edge has zero deflection. The bottom set of curves gives the components of mode shape for a value of c/s given by the tick mark on the second loop of the flutter boundary of figure 2. The effect of increasing the chord is to add more waves to the mode shape.

In the results discussed so far, the chordwise variations of deflections were allowed complete freedom and an exact solution was possible. In a practical case, an exact solution would not be feasible, and some sort of approximation of the chordwise deflection shape would be necessary. Some flutter boundaries obtained by approximating the chordwise deflections by the first few terms of a power series are shown in figure 4. The dashed curve gives the results for parabolic deformations, and the long-and-short-dashed curve gives the results for cubic deformations. The exact boundary is also shown for comparison. Both approximations yield good results for the lower values of c/s. The cubic approximation is almost exact. For longer chords, however, both approximations yield poor results. Apparently, in order to analyze the flutter behavior of wings in this range, higher order terms in the deflection shape must be used.

It can be seen from figure 2 that for each value of mass ratio a limiting value of the dynamic-pressure parameter can be obtained by considering the values at the bottom of the loops as the chord becomes large. The variation of this limiting value with mass ratio is shown in figure 5. The results obtained so far indicate that this curve gives a conservative estimate of the flutter speed for thin rectangular plates of very low aspect ratio. It should be noted that the flutter speed is less than the divergence speed and seems to approach it asymptotically for high mass ratio.

Several preliminary tests of some low-aspect-ratio plates at supersonic Mach numbers have been run in the Langley 9- by 18-inch supersonic flutter tunnel. The results of these tests are shown in figure 6. The flutter speed of the various models is shown as a ratio of experimental flutter speed to calculated flutter speed, where the calculated flutter speed was obtained from the curve in figure 5. This ratio is plotted against the ratio of chord to semispan. The agreement between theory and experiment is fairly good in view of the approximations inherent in the theory and of the preliminary nature of the tests.

During the tests the flutter modes were observed, and it was noted that the specimens with the larger ratios of chord to semispan had the more complicated mode shapes as is predicted by theory.

CONCLUDING REMARKS

The flutter analysis of low-aspect-ratio rectangular plates indicates that the flutter-mode shape has an increasing number of waves in the chordwise direction as the aspect ratio is reduced; approximating the chordwise deflection shape by parabolic or cubic curves yields flutter speeds in fair agreement with those of the more exact theory, provided that the aspect ratio is not too low. The cubic curve gives somewhat better results. For lower aspect ratios, higher order approximations must be used. Experimental data indicate that the flutter speed and the type of mode shape yielded by the theory are in fair agreement with experimental results.

Langley Aeronautical Laboratory,
National Advisory Committee for Aeronautics,
Langley Field, Va., March 7, 1957.

[redacted]

APPENDIX

ANALYSIS

In the application of slender-body aerodynamic theory to the present unsteady-flow problem, terms containing time derivatives in the velocity-potential equation for linearized flow are neglected in addition to those containing streamwise x-derivatives. The velocity-potential equation thus reduces to Laplace's equation in the crossflow plane. The boundary conditions on velocity and the pressure-potential relations are taken to be the same as those ordinarily used in unsteady linearized aerodynamic theory.

The potential φ and the aerodynamic loads resulting from the given deformation shape are calculated in a manner similar to that used in reference 1 for the static-divergence problem.

The principle of minimum potential energy is used to derive the differential equation of equilibrium for the function $F(x,\tau)$ in a manner analogous to that used in reference 1. Solution yields an eigenvalue equation which relates the flutter speed to the properties of the plate and the surrounding air:

$$0 = 64\alpha\beta\left[\left(D_1 \cos\frac{2\gamma c}{s} + E_1 \cosh\frac{\alpha c}{s}\cosh\frac{\beta c}{s} + \frac{F_1}{\alpha\beta}\sinh\frac{\alpha c}{s}\sinh\frac{\beta c}{s}\right) + i\left(D_2 \sin\frac{2\gamma c}{s} + \frac{E_2}{\alpha}\sinh\frac{\alpha c}{s}\cosh\frac{\beta c}{s} + \frac{F_2}{\beta}\cosh\frac{\alpha c}{s}\sinh\frac{\beta c}{s}\right)\right] \qquad (1)$$

where

$$i = \sqrt{-1}$$

$$D_1 = -\left[2A_1A_2 + A_1B_2 + A_2B_1\right]$$

$$E_1 = (A_3 + \lambda B_3)\left[2A_3 - (4\gamma^2 + \alpha^2 + \beta^2)A_4\right] + (A_4 - \lambda)\left[2\alpha^2\beta^2A_4 - (4\gamma^2 + \alpha^2 + \beta^2)A_3\right]$$

[redacted]

$$F_1 = (A_3 + \lambda B_3)\left[2\alpha^2\beta^2 A_4 - (4\gamma^2 + \alpha^2 + \beta^2)A_3\right] +$$

$$\alpha^2\beta^2(A_4 - \lambda)\left[2A_3 - (4\gamma^2 + \alpha^2 + \beta^2)A_4\right]$$

$$D_2 = -(A_1B_2 - A_2B_1)$$

$$E_2 = \gamma\left\{(A_3 + \lambda B_3)\left[\lambda\left(8\gamma^2 + 8a_1 - 8\lambda + \frac{K^2}{\gamma^2}\frac{5\epsilon}{12}\right) - 2(\gamma^2 - \lambda)\frac{K}{\gamma}\sqrt{\frac{5\epsilon\lambda}{12}}\right] -\right.$$

$$\left.\alpha^2(A_4 - \lambda)\left[\lambda\left(8\gamma^2 + 8a_1 - 8\lambda + \frac{K^2}{\gamma^2}\frac{5\epsilon}{12}\right) + 2(\gamma^2 - \lambda)\frac{K}{\gamma}\sqrt{\frac{5\epsilon\lambda}{12}}\right]\right\}$$

$$F_2 = -\gamma\left\{(A_3 + \lambda B_3)\left[\lambda\left(8\gamma^2 + 8a_1 - 8\lambda + \frac{K^2}{\gamma^2}\frac{5\epsilon}{12}\right) + 2(\gamma^2 - \lambda)\frac{K}{\gamma}\sqrt{\frac{5\epsilon\lambda}{12}}\right] -\right.$$

$$\left.\beta^2(A_4 - \lambda)\left[\lambda\left(8\gamma^2 + 8a_1 - 8\lambda + \frac{K^2}{\gamma^2}\frac{5\epsilon}{12}\right) - 2(\gamma^2 - \lambda)\frac{K}{\gamma}\sqrt{\frac{5\epsilon\lambda}{12}}\right]\right\}$$

in which

$$A_1 = -\frac{100}{9}(1 - \mu)^2 - \frac{10\mu}{3}\gamma^2 + \left(\gamma^2 - \lambda - \frac{K}{2\gamma}\sqrt{\frac{5\epsilon\lambda}{12}}\right)^2$$

$$A_2 = -\frac{100}{9}(1 - \mu)^2 - \frac{10\mu}{3}\gamma^2 + \left(\gamma^2 - \lambda + \frac{K}{2\gamma}\sqrt{\frac{5\epsilon\lambda}{12}}\right)^2$$

$$B_1 = \frac{20}{3}(1 - \mu)\lambda + (\gamma^2 - \lambda)\left(2\lambda + \frac{K}{\gamma}\sqrt{\frac{5\epsilon\lambda}{12}}\right)$$

$$B_2 = \frac{20}{3}(1 - \mu)\lambda + (\gamma^2 - \lambda)\left(2\lambda - \frac{K}{\gamma}\sqrt{\frac{5\epsilon\lambda}{12}}\right)$$

$$A_3 = \frac{100}{9}(1 - \mu)(1 - 2\mu) - \frac{20}{3}(1 - \mu)\lambda + \frac{10}{3}(1 - \mu)\gamma^2 + \lambda^2 - \frac{K^2}{4\gamma^2}\frac{5\epsilon\lambda}{12}$$

[redacted]

$$A_4 = \frac{10}{3}(1 - \mu) + \gamma^2$$

$$B_3 = \frac{10}{3}\mu - \gamma^2$$

$$\alpha^2 = \gamma^2 - 2(\lambda - a_1) + \frac{K}{\gamma}\sqrt{\frac{5\epsilon\lambda}{12}}$$

$$\beta^2 = \gamma^2 - 2(\lambda - a_1) - \frac{K}{\gamma}\sqrt{\frac{5\epsilon\lambda}{12}}$$

$$\frac{K^2}{\gamma^2} = \frac{4\left[\left(\gamma^2 - \lambda + a_1\right)^2 - 5\right]}{\frac{5\epsilon\lambda}{12} - \gamma^2\left(1 + \frac{5\epsilon}{12}\right)}$$

$$\lambda = \frac{5\pi}{4}\left(1 - \mu^2\right)\frac{q}{E}\frac{s^3}{t^3}$$

$$\epsilon = \frac{\pi}{2}\frac{\rho s}{\rho_m t}$$

$$K = \omega\sqrt{\frac{\rho_m t s^4}{D}}$$

$$a_1 = \frac{10}{3}\left(1 - \frac{3}{2}\mu\right)$$

In equation (1), α and β can be either real or imaginary quantities. Solution by trial yields the curves given in figure 2.

The divergence boundary obtained from reference 1 can also be obtained from the present analysis by setting the flutter-frequency parameter K equal to zero.

Mode Shapes

The flutter-mode shapes shown in figure 3 can be obtained from the following equation, where the real part gives the component in phase and

[redacted]

the imaginary part, the component out of phase with the maximum leading-edge deflection:

$$f(x) = \frac{C_1 e^{im_1 \frac{x}{s}} + C_2 e^{im_2 \frac{x}{s}} + C_3 e^{im_3 \frac{x}{s}} + C_4 e^{im_4 \frac{x}{s}}}{C_1 + C_2 + C_3 + C_4}$$

where

$$C_1 = \Big[(m_2 - m_4)(a_2 - m_3^2) A_{24} e^{-i(m_1+m_3)\frac{c}{s}} +$$

$$(m_3 - m_2)(a_2 - m_4^2) A_{23} e^{-i(m_1+m_4)\frac{c}{s}} +$$

$$(m_4 - m_3)(a_2 - m_2^2) A_{34} e^{-i(m_1+m_2)\frac{c}{s}} \Big]$$

$$C_2 = \Big[(m_3 - m_4)(a_2 - m_1^2) A_{34} e^{-i(m_1+m_2)\frac{c}{s}} +$$

$$(m_4 - m_1)(a_2 - m_3^2) A_{14} e^{-i(m_2+m_3)\frac{c}{s}} +$$

$$(m_1 - m_3)(a_2 - m_4^2) A_{13} e^{-i(m_2+m_4)\frac{c}{s}} \Big]$$

$$C_3 = \Big[(m_4 - m_2)(a_2 - m_1^2) A_{24} e^{-i(m_1+m_3)\frac{c}{s}} +$$

$$(m_1 - m_4)(a_2 - m_2^2) A_{14} e^{-i(m_2+m_3)\frac{c}{s}} +$$

$$(m_2 - m_1)(a_2 - m_4^2) A_{12} e^{-i(m_3+m_4)\frac{c}{s}} \Big]$$

[redacted]

$$C_4 = \left[(m_2 - m_3)\left(a_2 - m_1^2\right)A_{23}e^{-i(m_1+m_4)\frac{c}{s}} + \right.$$

$$(m_3 - m_1)\left(a_2 - m_2^2\right)A_{13}e^{-i(m_2+m_4)\frac{c}{s}} +$$

$$\left. (m_1 - m_2)\left(a_2 - m_3^2\right)A_{12}e^{-i(m_3+m_4)\frac{c}{s}} \right]$$

in which

$$m_1 = \gamma + i\beta$$

$$m_2 = \gamma - i\beta$$

$$m_3 = -\gamma + i\alpha$$

$$m_4 = -\gamma - i\alpha$$

$$A_{pq} = -4a_2a_3 - a_2\left(m_p^2 + m_pm_q + m_q^2\right) - 4a_3m_pm_q + m_p^2m_q^2$$

$$a_2 = \frac{10}{3}\mu$$

$$a_3 = \frac{10}{3}\left(1 - \frac{5}{4}\mu\right)$$

Approximate Solutions

The approximate analysis used parallels the analysis for divergence presented in reference 1. Cubic approximation of the chordwise variation of deflection results in the following complex determinant:

[redacted]

$$\begin{vmatrix} \left[A + 12K\sqrt{\frac{5c\lambda}{12}}\right] & \left[\frac{1}{2}A + 4\lambda\frac{s}{c} + 14K\sqrt{\frac{5c\lambda}{12}}\right] & \left[\frac{1}{3}A + \left(8\lambda + \frac{20}{3}\mu\right)\frac{s}{c} + 14K\sqrt{\frac{5c\lambda}{12}}\right] & \left[\frac{1}{4}A + (12\lambda + 10\mu)\frac{s}{c} + 14K\sqrt{\frac{5c\lambda}{12}}\right] \\ \left[\frac{1}{2}A\right] & \left[\frac{1}{3}A + \frac{40}{3}(1 - \mu)\frac{s}{c} + 12K\sqrt{\frac{5c\lambda}{12}}\right] & \left[\frac{1}{4}A + \left\{4\lambda + \frac{10}{3}(4 - 3\mu)\right\}\frac{s}{c} + 1\frac{\beta}{3}K\sqrt{\frac{5c\lambda}{12}}\right] & \left[\frac{1}{5}A + \left\{8\lambda + \frac{20}{3}(2 - \mu)\right\}\frac{s}{c} + 13K\sqrt{\frac{5c\lambda}{12}}\right] \\ \left[\frac{1}{3}A + \frac{20}{3}\mu\frac{s}{c}\right] & \left[\frac{1}{4}A + \frac{10}{3}(4 - 3\mu)\frac{s}{c} + 1\frac{4}{3}K\sqrt{\frac{5c\lambda}{12}}\right] & \left[\frac{1}{5}A + \left\{\frac{8\lambda}{3} + \frac{40}{9}(4 - 3\mu)\right\}\frac{s}{c} + 4\frac{s^3}{c^3} + 12K\sqrt{\frac{5c\lambda}{12}}\right] & \left[\frac{1}{6}A + \left\{6\lambda + \frac{20}{3}(3 - 2\mu)\right\}\frac{s}{c} + 6\frac{s^3}{c^3} + 1\frac{12}{5}K\sqrt{\frac{5c\lambda}{12}}\right] \\ \left[\frac{1}{4}A + 10\mu\frac{s}{c}\right] & \left[\frac{1}{5}A + \frac{20}{3}(2 - \mu)\frac{s}{c} + 1K\sqrt{\frac{5c\lambda}{12}}\right] & \left[\frac{1}{6}A + \left\{2\lambda + \frac{20}{3}(3 - 2\mu)\right\}\frac{s}{c} + 6\frac{s^3}{c^3} + 1\frac{8}{5}K\sqrt{\frac{5c\lambda}{12}}\right] & \left[\frac{1}{7}A + \left\{\frac{24}{5}\lambda + 8(3 - 2\mu)\right\}\frac{s}{c} + 12\frac{s^3}{c^3} + 12K\sqrt{\frac{5c\lambda}{12}}\right] \end{vmatrix} = 0 \quad (2)$$

where

$$A = \left[20 - K^2\left(1 + \frac{5\epsilon}{12}\right)\right]\frac{c}{s}$$

This equation was solved by trial to obtain the long-and-short-dashed curve in figure 4. The equation for parabolic deformation is obtained from equation (2) by omitting the last column and last row. The results for parabolic deformation are shown by the dashed curve of figure 4.

REFERENCE

1. Hedgepeth, John M., and Waner, Paul G., Jr.: Analysis of Static Aeroelastic Behavior of Low-Aspect-Ratio Rectangular Wings. NACA TN 3958, 1957.

[redacted]

CANTILEVER PLATE OF VERY LOW ASPECT RATIO

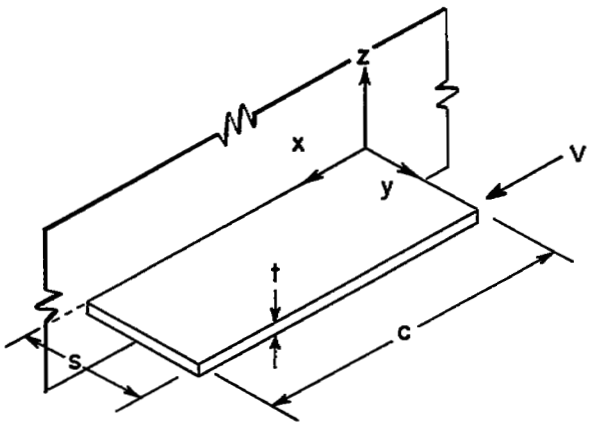

Figure 1

FLUTTER AND STATIC DIVERGENCE BOUNDARIES

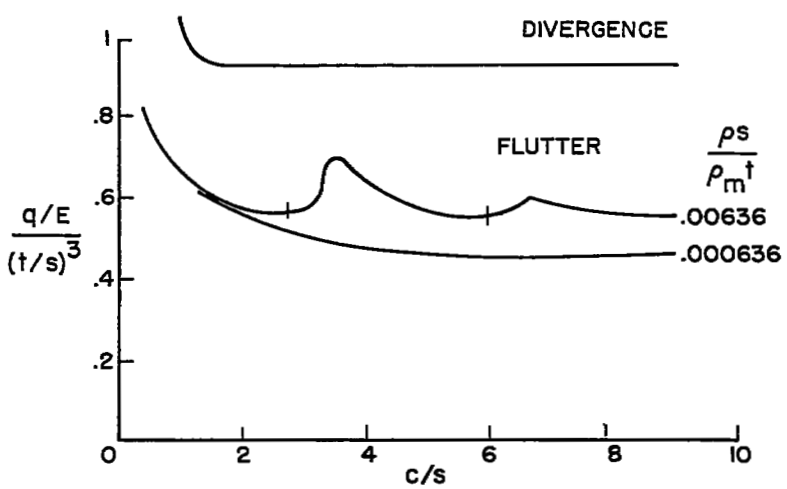

Figure 2

[redacted]

FLUTTER MODE SHAPES

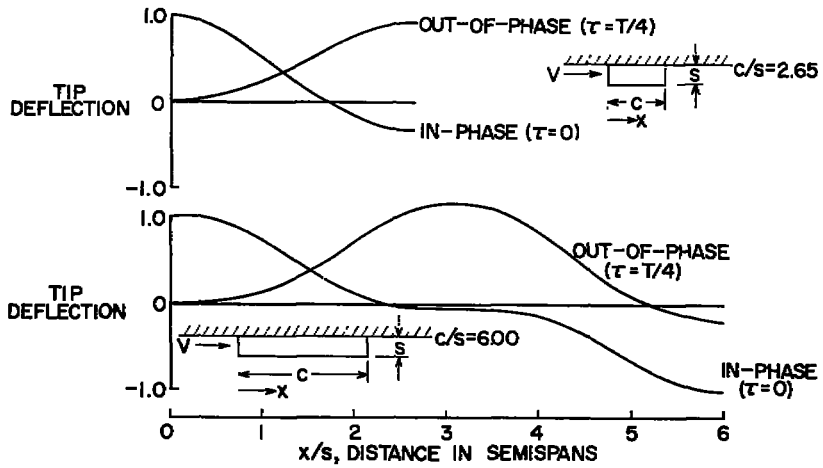

Figure 3

FLUTTER BOUNDARIES OBTAINED FROM APPROXIMATE DEFLECTION FUNCTIONS

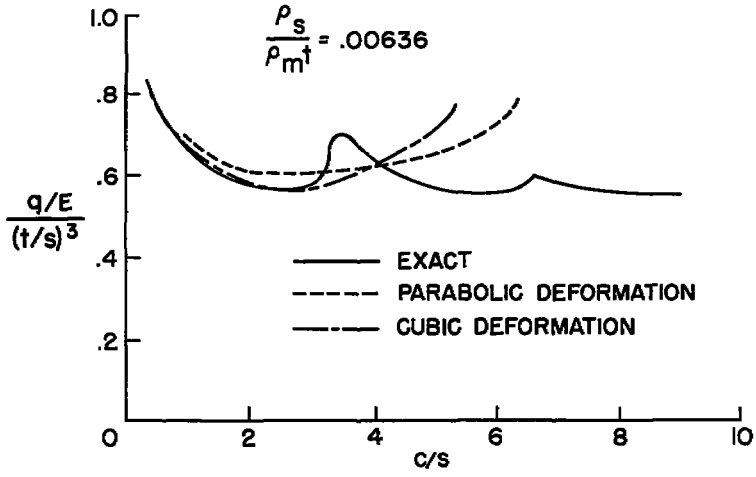

Figure 4

[redacted]

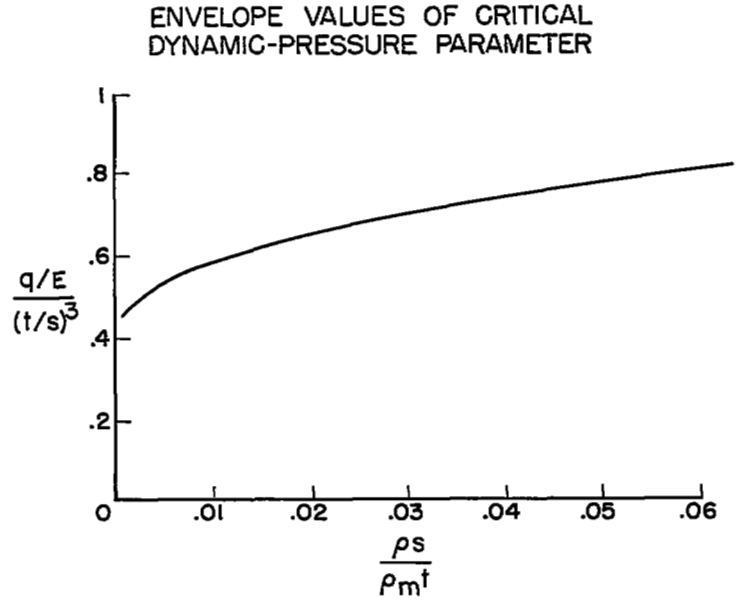

Figure 5

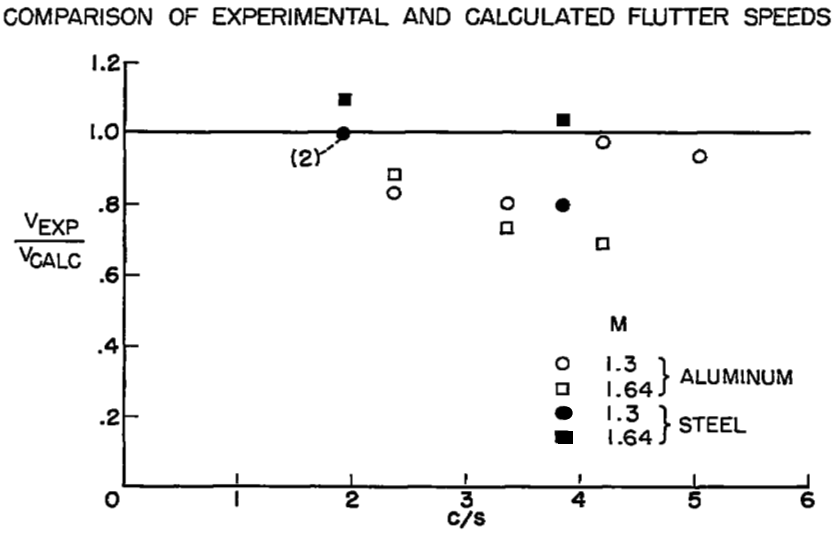

Figure 6

[redacted]